Nanosheet Exfoliation

DOI: 10.1002/ange.201308294

One-Step Exfoliation and Fluorination of Boron Nitride Nanosheets and a Study of Their Magnetic Properties**

Miao Du, Xianlei Li, Aizhu Wang, Yongzhong Wu, Xiaopeng Hao, and Mingwen Zhao**

Abstract: *A novel, simple, and efficient method for the preparation of the fluorinated hexagonal boron nitride nanosheets (F-BNNSs) and the corresponding magnetic properties is presented. A one-step route is used to exfoliate and fluorinate the BNNSs by ammonium fluoride (NH_4F) from hexagonal boron nitride (h-BN) powder. Through related instrument characterizations and theoretical calculations, we confirm that large-area and few-layer F-BNNSs were successfully produced by this method, which can be attributed to a fluorination-assisted exfoliation mechanism from the bulk h-BN in NH_4F. More intriguingly, we initially verified that the as-prepared F-BNNSs exhibit ferromagnetic characteristics, which would have good potential applications in spintronic devices.*

In recent years, graphene has received much attention owing to its unique properties and wide range of applications.[1–3] Hexagonal boron nitride nanosheets (BNNSs) are an analogue of graphene in which alternating boron and nitrogen atoms substitute for carbon atoms. In contrast to graphene, BNNSs have many distinct properties, such as high-temperature stability, intrinsic electrical insulation, and anti-oxidation ability.[4] As a result, BNNSs offer more innovative application perspectives than the bulk counterpart. For example, BNNSs can be used as a two-dimensional filler,[5] nonwetting coatings,[6] field emitters,[7] and an ideal substrate for high-quality graphene electronics.[8] However, the methods to prepare BNNSs are fewer and less effective than that of graphene, which is partially due to the stronger interactions among neighboring hexagonal boron nitride (h-BN) layers that make the exfoliation of BNNSs from bulk h-BN more difficult than peeling off graphene from graphite. In recent experimental studies, monolayer and few-layer BNNSs have been successfully prepared from bulk h-BN powder by the mechanical milling method,[9] chemical vapour deposition,[10,11] molten hydroxides method,[12] and chemical-solution-derived method.[13–15]

[*] M. Du, X. L. Li, A. Z. Wang, Prof. Y. Z. Wu, Prof. X. P. Hao, Prof. M. W. Zhao
State Key Lab of Crystal Materials, School of Physics
Shandong University, Jinan, 250100 (China)
E-mail: xphao@sdu.edu.cn
zmw@sdu.edu.cn

M. Du
Department of Chemistry
Qilu Normal University, Jinan, 250200 (China)

[**] This work was supported by National Basic Research Program of China (No. 2012CB932302), NSFC (Contract No. 91221101, 51321091), and IIFSDU (2012JC007).

Supporting information for this article is available on the WWW under http://dx.doi.org/10.1002/anie.201308294.

The published studies on the possible magnetic properties of fluorinated BNNSs (F-BNNSs) or boron nitride nanotubes (F-BNNTs) are of theoretical nature. For example, Li et al.[16] predicted that the chemisorption of fluorine atoms onto the boron atoms in BNNT can induce spontaneous magnetization. Zeng et al.[17] investigated the electron structure and the transport properties of fluorinated zigzag-edged boron nitride nanoribbons, showing that the transition between a half-metal and a semiconductor in the nanoribbons can be realized by fluorination at different sites or by changing the fluorination level. Kan et al.[18] demonstrated the possibility that single-layer BNNS can become ferromagnetic at room temperature and half-metallic upon fluorine adsorption. Zhang et al.[19] reported that fluorinating few-layered BNNSs could show a novel ferromagnetic spin state. Recently, there are literature reports of room temperature magnetism in BN.[20,21] For example, Song et al.[21] reported the observed ferromagnetism of the bulk BN in rhombohedra and hexagonal phases which arise from the conversion from sp^3 to sp^3–sp^2 hybridization as well as the unpaired spin electrons owing to defects. However, to the best of our knowledge, examining the magnetic properties of F-BNNSs has not been realized experimentally. Therefore, it is of crucial importance to develop a feasible method for synthesizing F-BNNSs and explore the corresponding magnetic properties.

Herein we present a novel, simple, and efficient method for the preparation of F-BNNSs and the corresponding magnetic properties. We have developed a one-step route to exfoliate and fluorinate the BNNSs by ammonium fluoride (NH_4F) from commercially available h-BN powder. This method has several advantages, such as having one step, a ready access to the raw materials, relatively high yields, mild reaction conditions, and low cost. At the same time, we propose a fluorination-assisted exfoliation mechanism to explain the formation of the F-BNNSs. The formation process involves the following sequence: fluorination, buckling of the sheets on the surface and insertion of ammonium ions, and exfoliation. More interestingly, through the related instrument characterizing, we verify that the as-prepared F-BNNSs exhibit clear ferromagnetic characteristics even at room temperture.

We first used scanning electron microscopy (SEM) to study the morphologies of as-obtained F-BNNSs. Figure 1 a–d shows the SEM images of the initial h-BN powder and F-BNNSs obtained using above mentioned method. The starting BN powder has representative lateral particle sizes in the range of 2–10 μm that are stacked together (Figure 1 a). As shown in Figure 1 b and c, the F-BNNSs have dimensions of several micrometers and are highly bent and scrolled, similar

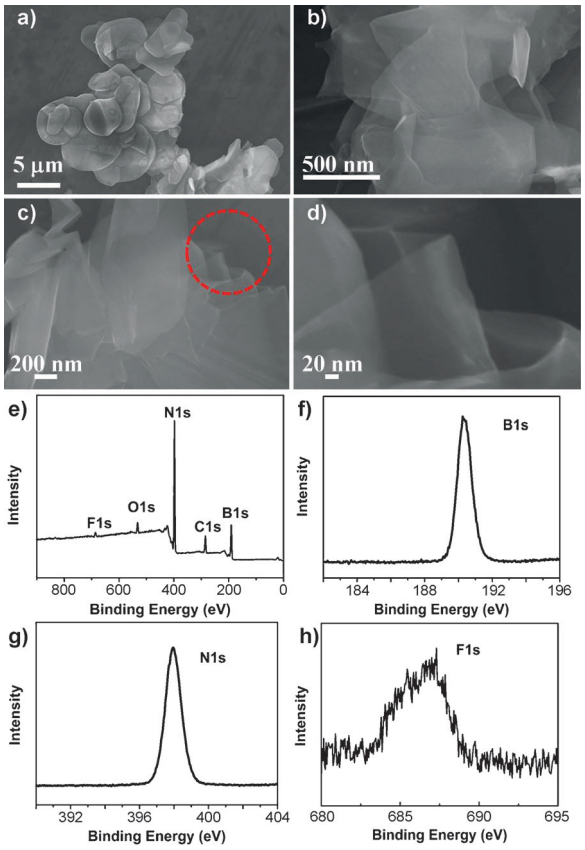

Figure 1. a) SEM image of initial h-BN powder. b),c) SEM images of F-BNNSs. d) Magnified SEM image of the region marked in (c) by a red circle. e) XPS survey spectrum of F-BNNSs. f) B 1s XPS spectrum of F-BNNSs. g) N 1s XPS spectrum of F-BNNSs. h) F 1s XPS spectrum of F-BNNSs.

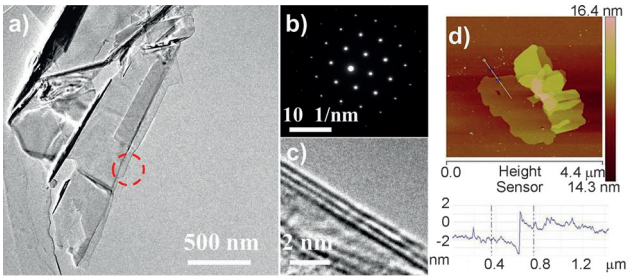

Figure 2. a) Low-magnification TEM image of F-BNNSs. b) Corresponding electron diffraction (ED) pattern of the region marked in (a) with a red circle, showing the hexagonal structure of BNNSs. c) High-resolution TEM image of the region marked in (a) with a red circle, consisting of three atomic layers. d) AFM image and corresponding height profile of F-BNNS.

to what has been reported for graphene.[22] The curling of F-BNNSs reduces the free surface and the dangling bond energy.[23,24] Compared with the initial h-BN powder, the size of F-BNNSs is smaller and the thickness is obviously reduced, which makes it almost transparent. Notably, as shown in Figure 1 d, the F-BNNSs became very thin and were peeled off layer-by-layer from the bulk h-BN.

To identify the chemical bonds and elemental composition of the F-BNNSs, we further characterized the products by X-ray photoelectron spectroscopy (XPS). Figure 1 e–h shows the XPS spectra of F-BNNSs. The intensity versus binding energy plots for B 1s, N 1s, and F 1s are shown in parts f, g, and h of Figure 1, respectively. The observed binding energy of B 1s, N 1s, and F 1s is 190.5, 397.9, and 686.9 eV, respectively. The measured values are in good agreement with reported values.[25,26] The B/N ratio from the XPS survey is 1.06, and the F/B ratio is about 0.02. Additional oxygen and carbon peaks shown in Figure 1 e most likely result from the exposure of F-BNNSs to air or during the XPS measurement preparation. It is noteworthy that if the F atoms attached only to the surface of the BNNSs, the compound would be too unstable to exist under beam irradiation in the electron microscope.[27,28] Therefore, we deduced that F atoms were covalently modified with some B atoms on the surface of BNNSs successfully. Furthermore, the FTIR and ^{19}F NMR characterization results also support this conclusion (see the Supporting Information for details).

High-resolution transmission electron microscopy (HRTEM) was then adopted to further analyze the F-BNNSs structure. Owing to the ultrathin shape, the F-BNNSs are almost transparent, as shown in Figure 2 a. From the image, it is clearly observed that the F-BNNSs are bent and scrolled with tapered edge morphology, consistent with the SEM images. The corresponding electron diffraction pattern (Figure 2 b) reveals the typical six-fold symmetry of h-BN, which demonstrates that the nanosheets are well-crystallized and not damaged during the synthesis process. Some nanosheets have curled edges, making it possible to determine the number of layers and thickness of these sheets by examining the edges. Figure 2 c reveals a F-BNNS edge with three layers and lattice distance that are deduced to be 0.33 nm, which indicates that the lattice fringes are the (002) crystal planes of h-BN. From this, we could infer that the exfoliation process occurred on the (002) plane of the bulk h-BN.

Atomic force microscopy (AFM) in the tapping mode was also employed to study the thickness and fine structure of the F-BNNSs, which was more accurately than that obtained by SEM and HRTEM characterization. Figure 2 d shows an isolated flat nanosheet that is similar in size to that observed in the HRTEM image (Figure 2 a). As shown in Figure 2 d, the thickness of the F-BNNSs is 1.514 nm. Previous reports showed that the AFM height of a BNNS monolayer increases to 1 nm owing to trapped solvents between the BNNS layer and the underlying substrate.[29] Thus, the number of layers deduced from the AFM data is less than three, which is in good agreement with the HRTEM data. In particular, the lateral size of the F-BNNSs is about 4 μm. Such large-area and few-layered F-BNNSs obtained through an one-step method have not been reported prior to this work.

Based on the structural characteristics of the synthesized F-BNNSs, we proposed a fluorination-assisted exfoliation mechanism (Figure 3) for h-BN in ammonium fluoride. This exfoliation process involves three stages: 1) F ions chemically bind to the B atoms on the surface of h-BN, making the B atoms sp^3-hybridized; the binding energy between F and B is

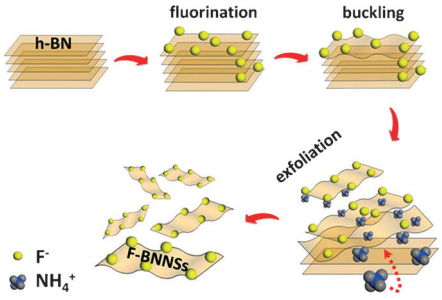

Figure 3. Illustration of the fluorination-assisted exfoliation mechanism. The exfoliating process involves the following sequence: fluorination, buckling of the sheets on the surface, insertion of ammonium ions, and exfoliation of sheets.

4.17 eV per bond, as revealed by first-principles calculations; the sp^3-hybridized B atoms extrude out of the basal plane of h-BN; 2) Driven by the sp^3-hybridized B atoms underlying F ions, the planar BN sheet begins to curl, leading to buckling of the outmost BN sheet; the buckling tendency overcomes the van der Waals (vdW) interactions between adjacent BN sheets, enlarging the interlayer spacing in some local regions (for example the edges), which facilities the intercalation of ammonium ions; 3) The diffusion of the intercalated ammonium ions exfoliates the F-BNNSs from the bulk h-BN; the curling morphology remains in the exfoliated F-BNNSs; this mechanism was also supported by other control experiments and first-principles calculations (see the Supporting Information for details).

The magnetic properties of the F-BNNSs were studied with a superconducting quantum interferometer device (SQUID) magnetometer from Quantum Design. Figure 4a shows the magnetization curves of raw materials (h-BN powder and NH_4F) and F-BNNSs at 5 K, after subtraction of the diamagnetic background. The magnetic hysteresis loops for F-BNNSs (triangles) in a low field from −1000 Oe to 1000 Oe exhibit clear ferromagnetic characteristics. The ferromagnetism is very weak, which is in consistent with the NMR result that the proportion of $F\text{-}BN_3$ that can induce the magnetic moment is very small (Supporting Information, Section 4). Apparently, the magnetic signals of h-BN powder (circles) and NH_4F (squares) are much weaker than that of F-BNNSs, as shown in Figure 4a. Thus, we conclude that the observed ferromagnetism in the F-BNNSs is induced by fluorination and the impurity from the raw materials can be ruled out. But even so, we cannot completely rule out other impurity origins. Figure 4b shows the magnetization curves of F-BNNSs, measured at temperatures ranging from 5 K to 350 K. The magnetic hysteresis loops measured in the low-field range are plotted in Figure 4c. Obviously, ferromagnetic behavior of the F-BNNSs is robust at this temperature range, except that the remanent magnetic moment (M_r) decreases with the increase of temperature. The normalized remanent magnetic moments $M_r/M_r(0)$ as a function of temperature for the sample are plotted in Figure 4d. For temperatures lower than 350 K, the temperature dependence of the magnetization can be described by spin-wave theory. The measured data (solid circles) can be fitted using a perturbation theory up to third order for spin-wave magnetization based on a uniaxially anisotropic 2D Heisenberg model[30,31] (dashed line). The ferromagnetic critical temperature T_c obtained from the spin-wave theory is about 637 K, which is much higher than room temperature. Considering that the spin-flip effect was not taken into account in the spin-wave theory, we also employed an Ising model to describe the temperature-dependent magnetic moments near the critical temperature.[32–34] It is clear that the spin-wave theory in conjunction with the Ising model fits the experimental data very well using the fitting parameters $T_c^{SW} = 1120$ K (spin-wave critical temperature), $\Delta = 0.01$ (the anisotropy constant), and $T_c = 580$ K (see the Supporting Information for details). Thus the ferromagnetic critical temperature $T_c \approx 580$ K is deduced for the synthesized F-BNNSs.

We also performed first-principles calculations within the density-functional theory to reveal the origination of the ferromagnetism in the F-BNNSs. Fluorination can induce

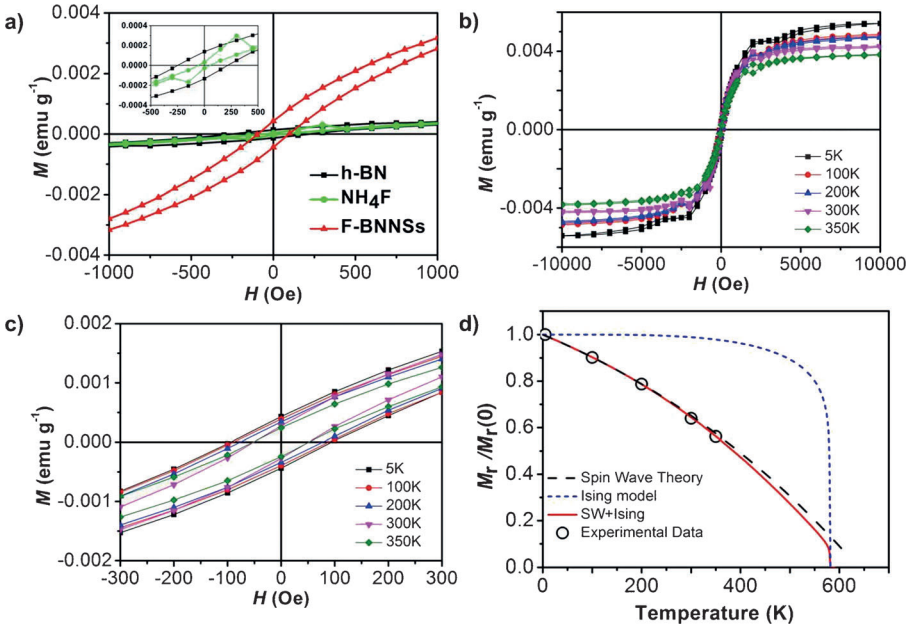

Figure 4. a) Hysteresis loops measured for raw materials and F-BNNSs for applied magnetic field between −1000 Oe and 1000 Oe. Inset: The enlarged hysteresis loops between −500 Oe and 500 Oe. b) The magnetization curves measured at temperatures ranging from 5 K to 350 K as a function of the applied magnetic field for the F-BNNSs. c) Low-field data. d) The normalized remanent magnetic moment as a function of temperature *T* measured for the sample, comparing the experimental data with the spin-wave theory in conjunction with the Ising model.

electron spin polarization in nonmagnetic BNNSs. The magnetic moment of F-BNNSs comes mainly from the electron spin-polarization of the F and the three N atoms nearest to the sp^3-hybridized B atom underlying the F atom. First-principles calculations also indicate that these local magnetic moments prefer to align ferromagnetically, forming long-range ferromagnetic ordering (see the Supporting Information for details). We therefore ascribe the ferromagnetism observed in the present experiments to the fluorination-induced electron spin-polarization in the F-BNNSs.

In summary, we have developed a one-step exfoliation and fluorination method to obtain F-BNNSs from the bulk h-BN. This method may be promising for large-scale synthesis. According to the experimental analysis, we proposed fluorination-assisted exfoliation mechanism from the bulk h-BN in ammonium fluoride. Furthermore, the as-prepared F-BNNSs exhibit obvious ferromagnetic characteristics, which is quite promising for applications in spintronic devices.

Experimental Section

Hexagonal boron nitride was purchased from Alfa Aesar. Ammonium fluoride, ethanol, *N*,*N*-dimethylformamide, N-methylpyrrolidinone, tetrahydrofuran, and chloroform (analytical reagent grade) were purchased from Kermel Reagent Co. Ltd.

In a typical experiment, h-BN power (0.2160 g) and ammonium fluoride (1.0200 g) was further ground into a homogeneous form and transferred in a Teflon-lined stainless steel autoclave. Deionized water (20 mL) was added and the system was heated at 180 °C for 24 h and then cooled down to room temperature. The autoclave container was taken out and the product was centrifuged and washed with ethanol and deionized water repeatedly until the pH of the supernatant was close to neutral. Finally, the as-obtained sample was dried in a vacuum oven for 24 h. About 44 mg of F-BNNSs could be obtained from 1 g of h-BN powder.

Scanning electron microscopy (SEM) images were obtained with a Hitachi S-4800 scanning electron microscope. High-resolution transmission electron microscopy (HRTEM) images were obtained with a Philips Tecnai 20U-Twin high-resolution transmission electron microscope at an acceleration voltage of 200 kV. The HRTEM samples were prepared by drying a doplet of the F-BNNSs ethanol suspension on a lacey carbon grid. Atomic force microscopy (AFM) images were obtained with a Nanoscope Multi Mode V (Digital Instruments/Bruker Systems), operating in Scan Asyst Air mode. The samples were prepared by depositing the F-BNNS ethanol suspension on a Si/SiO_2 substrate and dried in a vacuum oven for 12 h before AFM measurement. The X-ray photoelectron spectroscopy (XPS) was performed on an ESCALAB 2200-XL X-ray photoelectron spectrometer. Before and after fluorination, the magnetic moments of the sample assembly were measured at 5 K with a superconducting quantum interferometer device (SQUID) magnetometer from Quantum Design with a sensitivity of $\leq 10^{-7}$ emu. After fluorination, the SQUID measurements were performed at different temperatures, ranging from 5 K to 350 K, to examine the temperature dependence of the magnetic moments. FTIR spectra were carried out with a Thermo-Nicolet Nexus 670 infrared spectrometer. Raman spectra of the samples were obtained by the Lab RAM HR system of Horiba JobinYvon at room temperature using the 532 nm solid laser as the exciting source. ^{19}F solid-state magic angle spinning nuclear magnetic resonance (MAS NMR) spectra were recorded using a Bruker Avance III 400 MHz spectrometer.

Received: September 22, 2013
Revised: January 21, 2014
Published online: March 3, 2014

Keywords: boron nitride · exfoliation · ferromagnetism · fluorination · nanosheets

[1] K. S. Novoselov, A. K. Geim, S. V. Morozov, D. Jiang, Y. Zhang, S. V. Dubonos, I. V. Grigorieva, A. A. Firsov, *Science* **2004**, *306*, 666 – 669.
[2] Y. Zhu, S. Murali, W. Cai, X. Li, J. W. Suk, J. R. Potts, R. S. Ruoff, *Adv. Mater.* **2010**, *22*, 3906 – 3924.
[3] Z. S. Wu, W. Ren, L. Wen, L. Gao, J. Zhao, Z. Chen, G. Zhou, F. Li, H. M. Cheng, *ACS Nano* **2010**, *4*, 3187 – 3194.
[4] C. Zhi, N. Hanagata, Y. Bando, D. Golberg, *Chem. Asian J.* **2011**, *6*, 2530 – 2535.
[5] J. Taha-Tijerina, T. N. Narayanan, G. H. Gao, M. Rohde, D. A. Tsentalovich, M. Pasquali, P. M. Ajayan, *ACS Nano* **2012**, *6*, 1214 – 1220.
[6] A. Pakdel, C. Zhi, Y. Bando, T. Nakayama, D. Golberg, *ACS Nano* **2011**, *5*, 6507 – 6515.
[7] Z. G. Chen, J. Zou, *J. Mater. Chem.* **2011**, *21*, 1191 – 1195.
[8] C. R. Dean, A. F. Young, I. Meric, C. Lee, L. Wang, S. Sorgenfrei, K. Watanabe, T. Taniguchi, P. Kim, K. L. Shepard, J. Hone, *Nat. Nanotechnol.* **2010**, *5*, 722 – 726.
[9] L. H. Li, Y. Chen, G. Behan, H. Z. Zhang, M. Petravic, A. M. Glushenkov, *J. Mater. Chem.* **2011**, *21*, 11862 – 11866.
[10] Y. M. Shi, C. Hamsen, X. Jia, K. K. Kim, A. Reina, M. Hofmann, A. L. Hsu, K. Zhang, H. Li, Z. Juang, M. S. Dresselhaus, L. Li, J. Kong, *Nano Lett.* **2010**, *10*, 4134 – 4139.
[11] K. K. Kim, A. Hsu, X. Jia, S. M. Kim, Y. Shi, M. Hofmann, D. Nezich, J. F. Rodriguez-Nieva, M. Dresselhaus, T. Palacios, J. Kong, *Nano Lett.* **2012**, *12*, 161 – 166.
[12] X. Li, X. Hao, M. Zhao, Y. Wu, J. Yang, Y. Tian, G. Qian, *Adv. Mater.* **2013**, *25*, 2200 – 2204.
[13] Y. Lin, T. V. Williams, T. Xu, W. Cao, H. E. Elsayed-Ali, J. W. Connell, *J. Phys. Chem. C* **2011**, *115*, 2679 – 2685.
[14] C. Zhi, Y. Bando, C. Tang, H. Kuwahara, D. Golberg, *Adv. Mater.* **2009**, *21*, 2889 – 2893.
[15] M. Du, Y. Wu, X. Hao, *CrystEngComm* **2013**, *15*, 1782 – 1786.
[16] F. Li, Z. Zhu, X. Yao, G. Lu, M. Zhao, Y. Xia, Y. Chen, *Appl. Phys. Lett.* **2008**, *92*, 102515.
[17] J. Zeng, K. Chen, C. Sun, *Phys. Chem. Chem. Phys.* **2012**, *14*, 8032 – 8037.
[18] E. J. Kan, H. J. Xiang, F. Wu, C. Tian, C. Lee, J. L. Yang, M. Whangbo, *Appl. Phys. Lett.* **2010**, *97*, 122503.
[19] Z. Zhang, X. C. Zeng, W. Guo, *J. Am. Chem. Soc.* **2011**, *133*, 14831 – 14838.
[20] C. N. R. Rao, H. S. S. Ramakrishna Matte, K. S. Subrahmanyam, U. Maitra, *Chem. Sci.* **2012**, *3*, 45 – 52.
[21] B. Song, J. C. Han, J. K. Jian, H. Li, Y. C. Wang, H. Q. Bao, W. Y. Wang, H. B. Zuo, X. H. Zhang, S. H. Meng, X. L. Chen, *Phys. Rev. B* **2009**, *80*, 153203.
[22] N. G. Shang, P. Papakonstantinou, M. Mcmullan, M. Chu, A. Stamboulis, A. Potenza, S. S. Dhesi, H. Marchetto, *Adv. Funct. Mater.* **2008**, *18*, 3506 – 3514.
[23] L. M. Viculis, J. J. Mack, R. B. Kaner, *Science* **2003**, *299*, 1361.
[24] T. J. Booth, P. Blake, R. R. Nair, D. Jiang, E. W. Hill, U. Bangert, A. Bleloch, M. Gass, K. S. Novoselov, M. I. Katsnelson, A. K. Geim, *Nano Lett.* **2008**, *8*, 2442 – 2446.
[25] R. Trehan, Y. Lifshitz, J. W. Rabalais, *J. Vac. Sci. Technol. A* **1990**, *8*, 4026 – 4032.
[26] K. S. Lee, Y. S. Kim, M. Tosa, A. Kasahara, K. Yosihara, *Appl. Surf. Sci.* **2001**, *169*, 420 – 424.
[27] C. Tang, Y. Bando, Y. Huang, S. Yue, C. Gu, F. Xu, D. Gplberg, *J. Am. Chem. Soc.* **2005**, *127*, 6552 – 6553.

[28] H. J. Xiang, J. Yang, J. G. Hou, Q. Zhu, *Appl. Phys. Lett.* **2005**, *87*, 243113.
[29] Y. Lin, J. W. Connell, *Nanoscale* **2012**, *4*, 6906 – 6908.
[30] P. A. Serena, N. Garcia, A. Levanyuk, *Phys. Rev. B* **1993**, *47*, 5027 – 5036.
[31] A. P. Levanyuk, N. Garcia, *J. Phys. Condens. Matter* **1992**, *4*, 10277 – 10294.
[32] J. Barzola-Quiquia, P. Esquinazi, M. Rothermel, D. Spemann, T. Butz, N. Garcia, *Phys. Rev. B* **2007**, *76*, 161403.
[33] H. Xia, W. Li, Y. Song, X. Yang, X. Liu, M. Zhao, Y. Xia, C. Chen, T. W. Wang, D. Zhu, J. Gong, Z. Zhu, *Adv. Mater.* **2008**, *20*, 4679 – 4683.
[34] C. N. Yang, *Phys. Rev.* **1952**, *85*, 808 – 816.

